IJARSCT
International Journal of Advanced Research in Science, Communication and Technology
International Open-Access, Double-Blind, Peer-Reviewed, Refereed, Multidisciplinary Online Journal
ISSN: 2581-9429
Volume 6, Issue 1, July 2026
Impact Factor: 8.2

Performance Enhancement of Grid-Connected Solar PV Systems Using a TLBO-Tuned Fuzzy Nonlinear PI Controller

Deepak[1] and Anuradha Pathak[2]
Research Scholar, Department of Electrical Engineering, NITM, Gwalior, India[1]
Asst. Professor, Department of Electrical Engineering, NITM, Gwalior, India[2]

Abstract: *This research article presents a novel fuzzy-assisted nonlinear proportional-integral (f-NPI) controller based optimal power generation method for a 100 kW grid-connected solar photovoltaic (SPV) system with boost converter topology. The primary objective is to optimise power generation when variations in irradiance and temperature are experienced. f-PI and novel f-NPI based PV array reference current predictor is implemented to adjust the duty cycle for the converter. The gain parameters of controllers are being fairly tuned using teaching-learning based optimisation (TLBO) technique. A comprehensive simulation analysis is carried out using MATLAB R2017a, which verifies that the utilisation of primitive parameters, i.e., irradiance and temperature for the proposed controller exhibits enhanced performance in comparison to extant P&O and fuzzy logic controller (using secondary/conventional parameters like voltage and current) in terms of settling time, efficiency and THD. Moreover, the operation of the novel f-NPI based method is found to comply with IEEE 929 standard.*

Keywords: fuzzy system; solar photovoltaic system; renewable energy; grid-connected system; optimal power generation method; nonlinear controller; teaching learning-based optimization; TLBO; power efficiency; Perturb & Observe; P&O; total harmonic distortion; THD.

I. INTRODUCTION

A decrease in non-renewable resources such as natural gas, petroleum, coal, etc. adds fuel to the global problem of rising energy demand. As an act of grappling, alternative energy technologies are improving day by day. Among others, the best solution to this crisis is the use of renewable energy resources. The solar radiant energy accounts for most of the usable renewable energy on earth for the development of life. India has large solar energy potential with 300 clear days and 5,000 Petawatt/hours per year. The daily average solar energy incident over India varies from 4 kWh/m2 to 7 kWh/m2 with about 1,500–2,000 sunshine hour per year depending upon geographical terrain. At present, India is emerging as a fast-developing solar power industry, with total installed capacity reached to 33.75 GW in December 2019, 99.1 GWh of which got integrated into the national grid in 2017 (Chowdhury et al., 2020).

Some of the main advantages of utilising solar energy include unlimited resources, no harmful effect on the environment, a much better life cost cycle, and ease of accessibility in even remote areas where there is no electricity (Adhikari, 2018). However, the output of the PV array is dependent upon temperature and solar irradiance (Singh et al., 2020).

If these parameters fluctuate rapidly, then the output power of the PV array also fluctuates rapidly. For the extraction of optimal power and to cope up with the changing climaticconditions, the optimal generation using SPV array becomes a nonlinear problem. In addition to the maximisation of generated power output, an effective optimal method also enhances the power quality of the injected electrical energy into the grid terminals (Dash and Kazerani, 2010).

The optimal power generation process is conventionally initiated by sensing voltage and current of the PV array, which is then used to calculate the duty cycle or reference voltage for the DC-DC converter. Classical methods following this algorithm includes perturb and observe (P&O) (Sundareswaran et al., 2016) incremental conductance (INC) or hill-climbing techniques (Adhikari, 2018; Singh et al., 2020), constant voltage method, fraction short circuit current method, three-point weighted method, and ripple correlation method. These methods generally use fixed step size for tracking due to which, they have simple structures and are easy to implement with rapid convergence even for uniform shaded panel conditions. However, they have high oscillations around the optimal operating point. Many attempts were made to eliminate such disadvantages of classical algorithms by integrating conventional PI/PID controllers (Sahoo et al., 2018; Zhao et al., 2019). However, PID based classical power generation methods exhibit sluggish response with high settling time. To improve response, implementation of improvised PID based controllers including fractional-order PID (Kler et al., 2018b) and nonlinear PID controllers (Kler et al., 2018a) are examined on several platforms in recent studies. They provide fast response with high convergence rate; however, the results have also shown the inherent disadvantage of using improvised PID controllers along classical methods associated with low robust capabilities in terms of very high settling time.

For realising robust control when turbulent variations in atmospheric conditions are experienced, soft computing techniques are found to generate the optimal response. Various soft computing methods including fuzzy logic controllers (FLC) (Fannakh et al., 2019), artificial neural network (ANN) (Elobaid et al., 2015), particle swarm optimisation (PSO) (Renaudineau et al., 2015), and many other algorithms have been proposed for SPV based optimal power generation. In these techniques, input parameters are updated using variable step size perturbations until the optimal operating point is achieved. Among others, the fuzzy logic approach of furnishing response with higher precision under varying temperature and irradiance profile, without knowing the mathematical model of the understudy plant is well documented in the literature. Messai et al. (2011) is one such example that uses a fuzzy logic approach to estimate the optimum duty cycle for the DC-DC converter involved in the overall operating of the understudy system. The performance of the fuzzy logic-based optimisation method for such nonlinear plant is often found satisfactory and efficient (Francees and Elshafei, 2012). Therefore, fuzzy logic (FL) based approach is selected for implementation into this research article. While almost all soft computing technique utilises probabilistic reasoning due to which knowledge of the mathematical model becomes non-essential, on the other hand, their tracking efficiency substantially depends upon the accuracy of predicted input and output data. In Koizumi and Kurokawa (2005) the authors have compared conventional PID and fuzzy logic controllers (FLC) using combinations of different temperature and irradiance variations. The investigated simulation results show that the well-optimised PID controller has better performance than the conventional FLC method under the variable environmental conditions in terms of tracking optimal power generation state.

Model predictive control (MPC) techniques (Metry et al., 2017) is one of the advanced algorithms, where the control variables are used to obtain the optimised switching state based on the state-space model of the controlled system. However, the necessity of complex state-space models and fast computation blocks for the implementation of technique over a grid-interfaced moderate scale SPV system, makes the approach unfeasible for the understudy system (Huang et al., 2020). The authors in (Pathak and Yadav, 2019) had used a fuzzy logic-discrete PID (FL-DPID) controller to extract optimal power from a standalone PV system. The proposed controller in (Pathak and Yadav, 2019) is optimised using the genetic algorithm (GA) and uses PV array voltage and PV array current as inputs for the optimum duty cycle generation. However, optimising such parameters for each installation location is a non-feasible solution in real-world applications because of a wide range of operating voltage and current. Therefore, a new approach was necessary where robust capabilities of AI-based controllers to deal with variable environmental conditions can be practically adopted by a conventional controller like PID with superior overall efficiency.

Based on the literature survey, it can be concluded that while dynamic tracking efficiency of conventional non-AI based controllers is crucial, the robust capabilities of soft computing-based controllers also play important role in enhancing optimum power generation of the grid-connected PV system. Moreover, most of the above-mentioned

IJARSCT
International Journal of Advanced Research in Science, Communication and Technology
International Open-Access, Double-Blind, Peer-Reviewed, Refereed, Multidisciplinary Online Journal
ISSN: 2581-9429 Volume 6, Issue 1, July 2026 Impact Factor: 8.2

techniques use indirect parameters like PV array voltage and current, which results in a sluggish tracking response. These observations encouraged the authors for designing a cost-effective, novel optimal power generation algorithm that shares advantages of both, conventional and AI-based controllers with least dependency on the knowledge of system dynamics. Since the initial phases of research, the emphasis is given on selecting primitive variable parameters, i.e., solar irradiance and PV array surface temperature. After further investigation, it was analysed that the performance of the conventional PI controller could be further enhanced by considering the nonlinear nature of the dynamic error. It is realised by varying the integral gain of the conventional PI controller with a nonlinear function of error over the simulation time, which leads to the design of the NPI controller. Finally, the designed NPI controller is integrated into a fuzzy logic estimator resulting in the proposed fuzzy-assisted NPI (f-NPI) based optimal power generation algorithm. After the investigation of the proposed technique, it is observed that optimisation of the fuzzy logic membership function is now easily possible using a fundamental technique like the hit-and-trial method with much more accuracy and lesser time consumption than in the case of the fuzzy logic controller (FLC) based control algorithm.

II. SYSTEM DESCRIPTION

The understudy grid-connected SPV system with boost DC-DC converter-based topology (as shown in Figure 1) can be segregated into the following mutually exclusive subsystem for better understanding:

1 PV array
2 PV-side/ DC-DC converter and control
3 Grid-side inverter and control
4 transmission network and utility grid

In the understudy system, while the PV array acts as an energy source, a DC-DC boost converter is responsible for stepping up voltage of the panel power, transforming it into an upscale form, more suitable for operation at following subsystems. A three-phase, three-level voltage source converter (VSC) is not only responsible for transforming the DC-link PV power into AC, but it also ensures synchronism and unity power factor throughout the generation. At last, a transmission network including passive filters and compensators improves the power quality before feeding it to a local utility grid (Xavier et al., 2018). For understanding the overall system with efficient operation, modelling, and control methods of relevant models of the investigated system are being discussed in detail in the following sections.

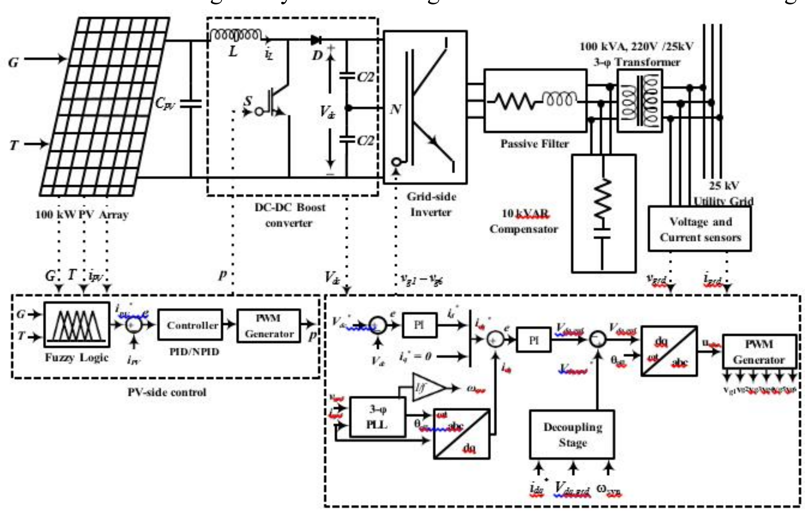

Figure 1 Understudy grid-connected PV system block-diagram

ISSN: 2581-9429
Volume 6, Issue 1, July 2026
Impact Factor: 8.2

2.1 PV array modelling

A solar cell is the basic building block of the solar PV (SPV) array. Solar cells are semiconductor p-n junctions operating under photoelectric effect, according to which, emitted light can be directly converted into electrical energy. The equivalent circuit of a solar cell as shown in Figure 2(a), consists of a current source with diode in parallel representing nonlinear resistance of p-n junction, along with intrinsic series resistance Rse and parallel resistance Rsh (Awadallah, 2016). Usually, the value Rsh is taken large whereas that of series resistance is taken small. PV cells are united together to form a larger unit called PV modules. These modules are further connected in series-parallel to achieve a higher power rating from a resultant PV array to generate electricity. Table 1 entails the parameters of the PV array considered in this study. Mathematically, fundamental equation (1) from the theory of semiconductors describes the V-I characteristics for a single diode model of ideal PV cell shown in Figure 2(b) (Singh et al., 2020).

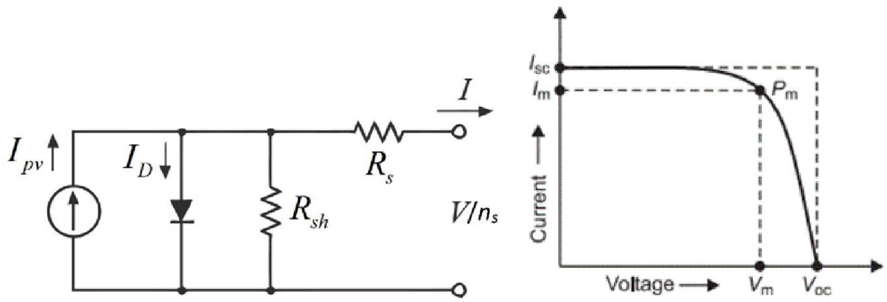

Figure 2 (a) Equivalent circuit (b) I-V characteristics of SPV cell

Table 1 SunPOWER 305E-WHT-U-PV solar array

Parameters	Values
Rated power	100.7 kW
Cells per module (ncell)	96
Series connected (ns)	5
Parallel strings	66
Open circuit voltage (Voc)	321 V
Voltage at optimal point with 1,000 W/m2, 25°C (Vmp)	273.5 V
Short-circuit current (Isc)	393.36 A
Current at optimal point with 1,000W/m2, 25°C (Imp)	368.28 A

$$I_{pv,cell} = I_{ph,cell} - I_{o,cell}\left(e^{\frac{qV_{oc}}{akT}}\right) \quad (1)$$

where IPV,cell represents the current generated by PV cell, the current generated by PV cell due to the corresponding irradiance or photocurrent IPh,cell, while the second part represents the Shockley diode equation. Photocurrent IPh,cell and the reverse saturation or leakage current of diode Io,cell, can be expressed as in equations (2) and (3), respectively:

$$I_{ph} = \frac{G}{1000}\left[I_{sc} + K_i(T - T_r)\right] \quad (2)$$

$$I_o = I_{or}\left(\frac{T}{T_r}\right)^3 e^{\left[\frac{qE_g}{aK}\left(\frac{1}{T_r}-\frac{1}{T}\right)\right]} \quad (3)$$

DOI: 10.48175/IJARSCT-37663

ISSN 2581-9429 IJARSCT

IJARSCT
International Journal of Advanced Research in Science, Communication and Technology
International Open-Access, Double-Blind, Peer-Reviewed, Refereed, Multidisciplinary Online Journal
ISSN: 2581-9429 Volume 6, Issue 1, July 2026 Impact Factor: 8.2

where q0 is the charge of an electron (= 1.6021 × 10^{-19} C), K is the Boltzmann's constant (= 1.3806503 × 10^{-23} J/K), Tr is the temperature of p-n junction (in K), and A is the diode ideality factor, Voc is the open-circuit voltage of cell and T is the temperature of the cell. The open-circuit voltage Voc and terminal voltage V of the PV cell can be expressed in equations (4) and (5), respectively.

$$V_{oc} = V + n_s IR_s \tag{4}$$

$$V = \frac{n_s AkT}{q_o}\ln\left(\frac{I_{ph} - I_o - I}{I_o}\right) - n_s IR_s \tag{5}$$

where I is module output current, Ic and Vc are cell output current and voltage, respectively, Iph and Vph are generated current and voltage, respectively, Isc and Io are short-circuit current and saturation current, respectively, Rs is module series resistance (in Ω), kT (=0.0017 A°/°C) is the short-circuit current temperature coefficient, G is irradiation in W/m2. The module power output power can be determined from equation (6):

P = V .I (6)

2.2 Boost DC-DC converter

The DC-DC boost converter is widely used in power systems when the input voltage in a particular section is needed to be stepped up to the operational limits. As shown in the operational diagram of the boost converter (Figure 3), during the switch ON, the inductor current flows through L and S, and during switch OFF, it flows through L, D, and the load, while the capacitor charges as shown in Figures 3(a)–3(b). In practice, a large input capacitor is generally connected between PV terminals and boost converter, whose critical value can be determined using expression (7) (Mumthas, 2018).

$$C_{pv} = \frac{I_{pv}}{f_{sw}\Delta V_{pv}} \tag{7}$$

where fsw is the sampling frequency and ΔVpv is the ripple in PV array output voltage. The output voltage for this converter in continuous conduction mode is given by equation (8).

Figure 3 DC-DC boost converter equivalent circuit during, (a) switch ON (b) switch OFF

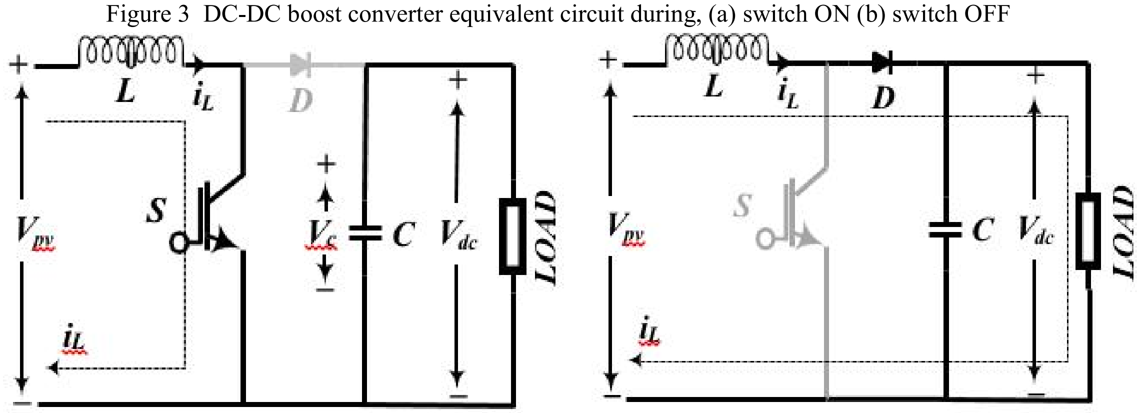

$$\frac{V_o}{V_i} = \frac{1}{1-D} \tag{8}$$

IJARSCT

International Journal of Advanced Research in Science, Communication and Technology

International Open-Access, Double-Blind, Peer-Reviewed, Refereed, Multidisciplinary Online Journal

ISSN: 2581-9429 Volume 6, Issue 1, July 2026 Impact Factor: 8.2

The critical value of inductance for the boost converter can be computed using equations (8)–(10):

$$i_{L\max} = \frac{P_O}{V_{in}} \tag{9}$$

$$L_{\min} = \frac{V_{in} D}{f_{sw} \Delta i_L} \tag{10}$$

where ΔiL is the peak-to-peak value of the inductor ripple current [Kazimierczuk, (2008), p.93]. The expressions required for computation of critical value corresponding to output capacitance is given by equation (11):

$$C_{\min} = \frac{V_O D}{f_{sw} R_L v_{cpp}} \tag{11}$$

where vcpp is the maximum peak-to-peak value of the ac component of the voltage across capacitance C and is the output shunt resistance of the converter. The final line-to-output transfer function of the boost converter in the continuous-time domain can be expressed as in equation (12) (Chen, 2013):

$$\frac{v_o}{v_{in}} = \frac{(1-D)}{(LC)s^2 + \left(\frac{L}{R}\right)s + (1-D)^2} \tag{12}$$

While calculating critical and then actual values of Cpv, L, and C, the following assumption were taken:

1 PV array ripple voltage ΔVpv can be assumed to be 30% of the DC-DC converter output voltage.

2 Ripple in inductor current ΔiL can be assumed to be less than 5% of the maximum output current.

3 Ripple in output voltage Vr can be assumed to be less than 1% of the output voltage, while vcpp amplitude can be assumed to be half of that of ripple voltage.

With all the above assumptions taken under consideration, the calculated values of fundamental electric components used in designing a boost converter for the understudy system are listed in Table 2.

Table 2 Boost- DC-DC converter relevant parameters

Parameters	*Values*
Input voltage (V_{in})	273.5 V (= V_{mp})
Input current (I_{in})	368.3 A (= I_{mp})
Output power (P_o)	100.7 kW
Output voltage (V_O)	500 V (= V_{dc})
Switching frequency (f_{sw})	5 kHz
Input capacitance (C_{pv})	900 μF
boost inductance (L)	1.5 mH
Output capacitance (C)	8 mF

2.3 Grid side control

A grid side converter (GSC) control module is used to provide synchronism between the inverter output terminal and the grid by ensuring constant voltage and frequency throughout the bus, while simultaneously ensuring unity power factor throughout the generation. It consists of a DC-link Capacitor, a 3-phase, 3-level VSC and a passive RL-based filter. The active and reactive power fed to the filter in dq reference frame, which can be used to implement the GSC system control model, is given by equations (13) and (14), respectively (Malakondareddy et al., 2019):

$$P = \frac{3}{2}\left(u_{d,grd} i_{d,grd} + v_{q,grd} i_{q,grd}\right) \quad (13)$$

$$Q = \frac{3}{2}\left(u_{q,grd} i_{d,grd} - u_{q,grd} i_{q,grd}\right) \quad (14)$$

For unity power factor operation, the d-axis synchronised grid voltage should be perfectly aligned along with the DC-link capacitor voltage, i.e., the q-axis synchronised grid voltage must become zero. With vq,grd = 0, equations (13) and (14) can be reduced to equations (15) and (16), respectively:

$$P = \frac{3}{2}\left(u_{d,grd} i_{d,grd}\right) \quad (15)$$

$$Q = -\frac{3}{2} u_{d,grd} i_{q,grd} \quad (16)$$

From equations (15) and (16), it is evident that the power fed into the grid depends upon reference values of id and iq components of currents, respectively. The active power reference current component id,grd* is generated by an outer voltage loop, responsible to control DC-Link voltage (ud,grd = Vdc = 500 V). Also, to minimise reactive power requirement or Q* = 0, the reactive power reference current component id,grd* must be kept zero as well. After obtaining reference current components, it is then fed into an inner current loop, controlling current components using a PI controller. The output of the inner current loop gives voltage Vdq,grd equivalent to current components. It is then fed into an inner current loop, controlling current components using a PI (Manaullah et al., 2017). The output of the inner current loop gives voltage Vdq,grd equivalent to current components of active and reactive power. These voltages are then used to obtain reference dq-frame voltages udq,grd* by controlling them close to their respective decoupled dq-frame voltages given in equations (17) and (18):

$$V_{d,grd}^{*} = v_{d,grd} - \omega_{syn} L_f i_{q,grd} \quad (17)$$

$$V_{q,grd}^{*} = v_{q,grd} + \omega_{syn} L_f i_{d,grd} \quad (18)$$

Converter reference voltages udq,grd* are then transformed to abc reference frame via inverse park's transformation equations using angle obtained via a 3-phase PLL, which is then finally fed to the PWM pulse generator to generate gating pulses for VSC.

2.4 Transmission network and utility grid

To ensure high power quality at the grid end, an RL-based passive filter is connected in between the inverter output terminal and grid (Adhikari et al., 2015). The generated power after being synchronised to the grid is first fed to a 100 kVA, 260V/25 kV, 3-phase transformer. It raises the generated power voltage level to the grid-level before it could be fed into the grid. A 10 kVAR compensator is connected in between to regulate the power quality throughout the generation.

III OPTIMAL POWER GENERATION METHODS

As could be observed from I vs. V and P vs. V curves of a PV array as shown in Figure 4 and Figure 5, the output of the solar panel depends on the varying solar irradiance, panel temperature, and other environmental conditions like humidity, etc., due to which the power generated throughout the day is not constant. Furthermore, there are certain naturally occurring phenomena like wind flow, rainfall, cloud movement, etc. due to which turbulence in the irradiance

IJARSCT
International Journal of Advanced Research in Science, Communication and Technology
International Open-Access, Double-Blind, Peer-Reviewed, Refereed, Multidisciplinary Online Journal
ISSN: 2581-9429
Volume 6, Issue 1, July 2026
Impact Factor: 8.2

and temperature profile could be observed while traversing through different seasonal variations of the Indian climate (Magare et al., 2016). As a result, the PV curve has multiple optimal power points, making the implementation a complex nonlinear problem. An important factor in deciding the efficiency of an SPV system is how well-associated control is designed to predict optimal power accurately. The main objective of this method is to operate the PV system close to its optimal power point under varying atmospheric conditions and/or load.

Figure 4 (a) I vs. V and (b) P vs. V curves of simulated Solar PV array when the temperature is constant (see online version for colours)

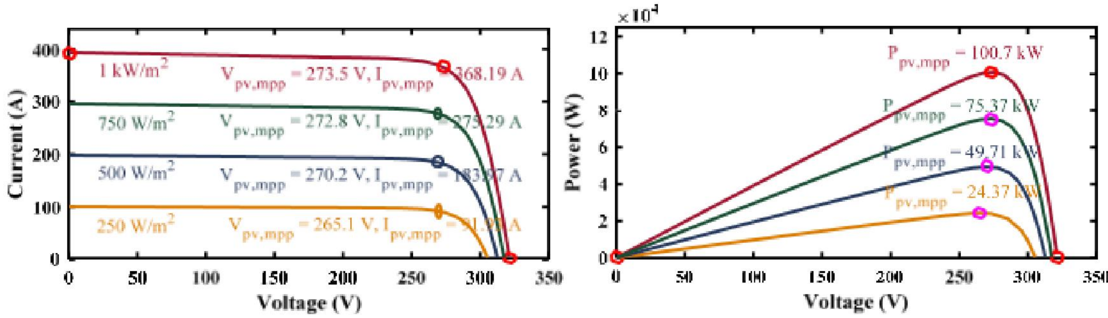

In addition to the optimal power generation, these methods also have a significant impact on the power quality of the generated electrical energy at the grid terminals. To explore this fact, we can observe the AC side of the inverter, from where the equation (19) can be deduced as:

$$L_f \frac{di_{abc,grd}}{dt} = v_{GSC} - v_{abc,grd} \qquad (19)$$

where Lf is the series inductance of the passive filter and iabc,grd, vabc,grd are the instantaneous values of grid currents and voltages respectively. The average output voltage of the GSC (vGSC) could be expressed in terms of DC-link voltage (Vdc) and duty cycle output of the optimal power generation method (D), using equation (20):

$$v_{GSC} = DV_{dc} \qquad (20)$$

The above expression indicates that the oscillations in the duty cycle and the output voltage of the boost converter due to inferior optimal methods leads to severe harmonic content in the inverter average output voltage which in turn gets injected into grid currents as per equation (19) (Salem and Atia, 2015). Figure 6 shows the comparative line-to-output time responses of the understudy boost converter [referring equation (12)] in the presence and absence of the proposed optimal power generation method respectively. The time-domain analysis is carried out with irradiance and temperature input kept constant at 1,000 W/m2 and 25°C respectively. As expected, the time response of the converter without controller is having large settling time and oscillations in comparison to the time response in the presence of the controller.

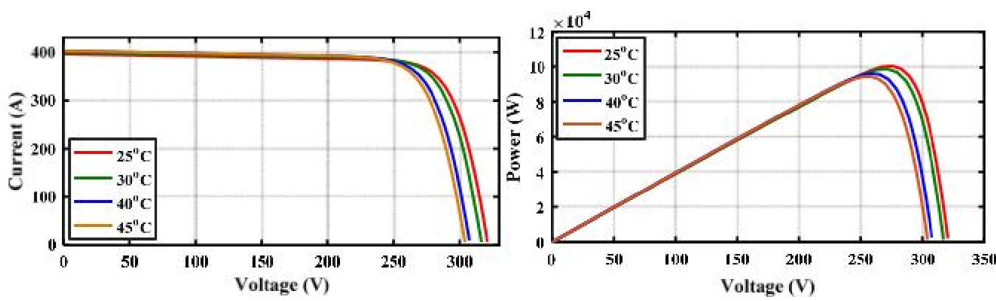

Figure 5 (a) I vs. V and (b) P vs. V curves of simulated SPV array when the temperature is varied (see online version for colours)

To predict the duty cycle accurately, there are some benchmark techniques in the literature such as perturb and observation (P&O), incremental conductance (INC) method, short-circuit current (SC) method etc. which shows good results in terms of circuit complexity, lesser metrics and tracking efficiency without a change in the atmospheric conditions. However, under the fast-changing atmospheric conditions, these algorithms lack the speed and adaptability to predict optimal power. Moreover, various intelligent methods, as discussed in the literature survey are available, which consider the turbulent atmospheric condition. In the following sections, extant as well as proposed strategies are modeled and discussed in detail.

3.1 Perturb and observe algorithm

This extant method is based on a hill-climbing search approach. It introduces small change (or perturb) in the duty cycle of the converter, controlling the operating DC-link voltage between the PV array and the power converter. If there is change (either increment or decrement) in the PV array power, the perturbation should keep in the same direction. The conventional P&O algorithm is developed based on the slope (dP/dV) variation on the P-V characteristics curve of the PV module (Singh et al., 2015). From the same shown in Figure 7, it can be observed that the slope is positive at the left and negative at the right of optimal power point. Depending on the sign of the slope, the duty cycle has to be perturbed in order to predict the peak/optimum power. This algorithm has less time and implementation complexity. In this technique, choosing the step size based on the grid and load base is a critical and cumbersome task. With unoptimised step size, it often results in oscillations, especially when abrupt variations in irradiance are experienced.

Figure 6 Time response of boost converter with and without optimal power generation method at normal operating condition (irradiance = 1,000W/m2; Module temperature = 25°C)
(see online version for colours)

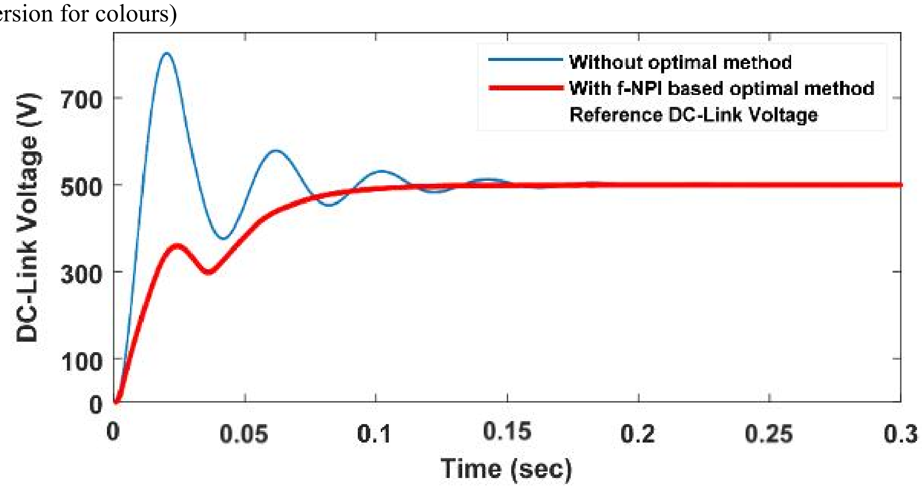

Figure 7 P-V curve with perturbation around operating point 2 (see online version for colours)

3.2 Adaptive fuzzy logic controller-based optimal power generation

Over the past few decades, advancements in the capabilities of microcontrollers have led many researchers to shift their focus to artificial intelligence (AI) for the development of novel control methods related to a variety of industrial automation processes. A fuzzy logic controller (FLC) is proven to have several advantages over other intelligent controllers including simple design, faster and accurate response time, even when imprecise inputs are involved. Another reason for its popularity among several branches of engineering is that they do not require a precise mathematical model of the system to handle nonlinearity.

Figure 8 FLC scheme for optimal power technique in the PV system (see online version for colours)

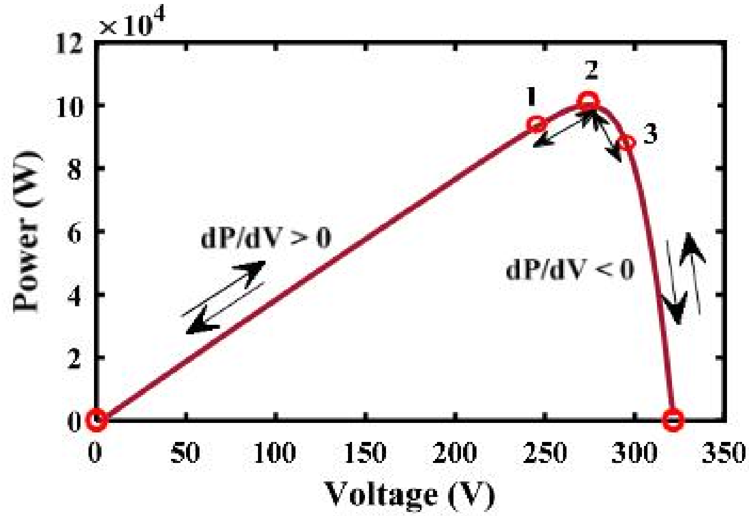

Figure 8 represents one of the simplest implementations of a fuzzy logic-based optimal power generation algorithm. The output of this controller provides a DC-DC converter duty cycle (D) which is then transformed into switch's gate pulses when fed through a pulse width modulation (PWM) generator. The proposed method in Rezk et al. (2019) utilises the working principle of the conventional P&O technique as the inputs of the Adaptive-FLC (AFLC) are the absolute and rate of change values of the error signal, expressed as equations (21) and (22):

$$e = \frac{P_{pv}(n) - P_{pv}(n-1)}{V_{pv}(n) - V_{pv}(n-1)} \tag{21}$$

$$\Delta e = e(n) - e(n-1) \tag{22}$$

where , and , are the discrete samples of current and previous PV array terminal power and voltage respectively. For ease in processing, the crisp inputs are mapped into fuzzy sets using seven fuzzy membership functions with linguistic variables: very negative (VN), moderate negative (MN), small negative (SN), zero (Z), small positive (SP), moderate positive (MP), and very negative (VN). Once the fuzzified inputs are computed, a Fuzzy-logic inference engine predicts the duty cycle (D) of the boost converter based on 49 (= 7 × 7) distinct rules and output membership functions with seven linguistic variables: extra small (XS), very small (VS), small (S), medium (M), long (L), very long (VL), and extra long (XL). As inputs, the output of the inference engine is defined within the fuzzy set. Hence, a defuzzification unit revert the fuzzy output into the crisp values of the duty cycle required to obtain optimal operational point based on current magnitudes of PV terminal voltage and power. Please note that the variation in the duty cycle will be observed until the optimal voltage and current is established. Afterward, the duty cycle will attain a constant value corresponding to optimal (Vpv*) and reference DC-link voltage (Vdc*). A detailed implementation of the extant algorithm on the MATLAB/Simulink platform is shown in Figure 9. The membership functions and rule-base defined to estimate the duty cycle are summarised in Figure 10.

IJARSCT
International Journal of Advanced Research in Science, Communication and Technology
International Open-Access, Double-Blind, Peer-Reviewed, Refereed, Multidisciplinary Online Journal
ISSN: 2581-9429
Volume 6, Issue 1, July 2026
Impact Factor: 8.2

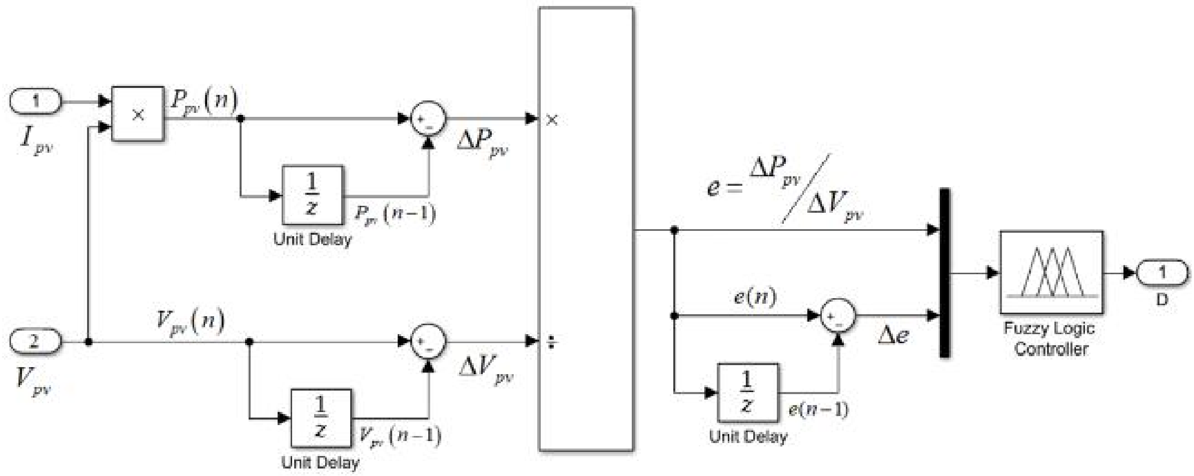

Figure 9 Adaptive fuzzy-logic controller (AFLC) optimal power control implementation in MATLAB/Simulink

The adaptation capabilities of the extant controller over a wide range of operating irradiance and temperature is one of the major factors due to which the industrial pioneers favour AI-based techniques implementation in real-world SPV applications. Unfortunately, the optimal point tracking performance of a conventional fuzzy-based controller is solely dependent upon the membership functions and the rule base defined according to the characteristics of the simulated PV module. Hence, these controllers are observed with inferior convergence rate in comparison to the hybrid fuzzy-PI/PID based techniques. Furthermore, due to the aforementioned reasons, a large number of rules and membership functions are required to ensure reliable, robust, and non-oscillatory performance throughout the operational time duration.

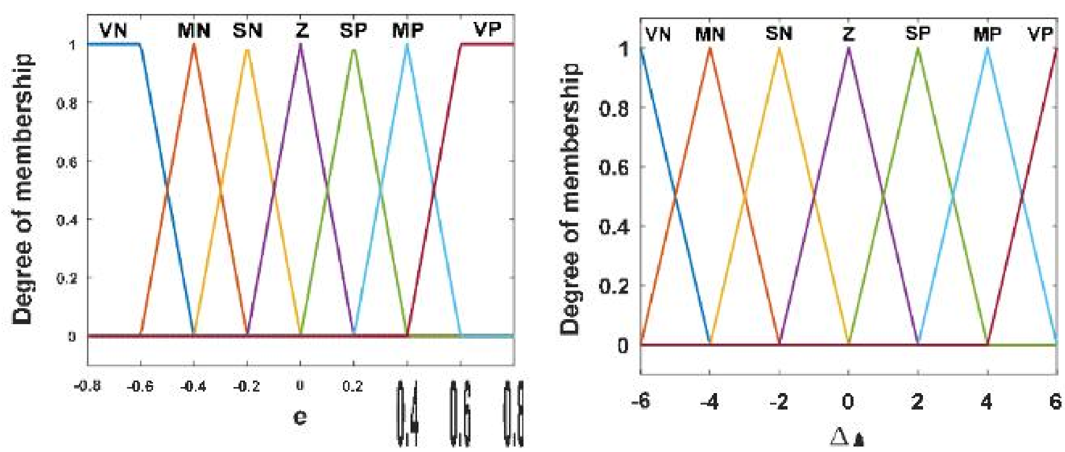

Figure 10 AFLC-based controller membership functions of, (a) PV array voltage [input] (b) PV array current [input] (c) PWM duty cycle [output] (d) rule base (see online version for colours)

DOI: 10.48175/IJARSCT-37663

IJARSCT
International Journal of Advanced Research in Science, Communication and Technology
International Open-Access, Double-Blind, Peer-Reviewed, Refereed, Multidisciplinary Online Journal
ISSN: 2581-9429 Volume 6, Issue 1, July 2026 Impact Factor: 8.2

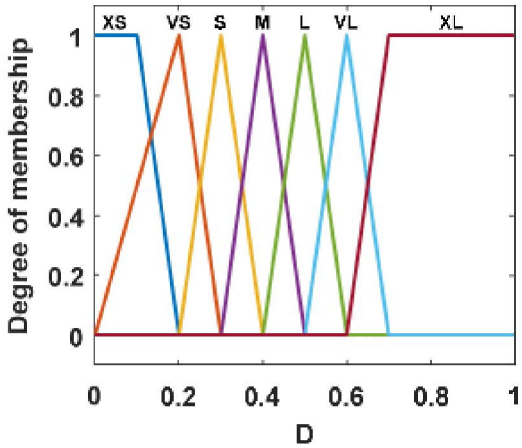

e	Δe						
	VN	MN	SN	Z	SP	MP	VP
VN	M	M	M	XS	XS	XS	XS
MN	M	M	M	VS	VS	VS	VS
SN	S	M	M	S	S	S	S
Z	VS	S	M	M	M	L	VL
SP	VL	L	L	M	M	M	M
MP	VL	VL	VL	M	M	M	M
VP	XL	XL	XL	M	M	M	M

Figure 10 AFLC-based controller membership functions of, (a) PV array voltage [input] (b) PV array current [input] (c) PWM duty cycle [output] (d) rule base (continued) (see online version for colours)

IV PROPOSED FUZZY ASSISTED OPTIMAL POWER GENERATION TECHNIQUE

The proposed power controller as shown in Figure 11, uses a Fuzzy-based algorithm with inputs:

1 irradiance, G

2 temperature, T.

The output of the fuzzy system is PV array reference current I* , which is then compared with the instantaneous PV array current Ipv. The error generated is then fed to a non-AI based controller to predict the duty cycle for the boost DC-DC converter.

Figure 11 Proposed controllers Simulink implementation

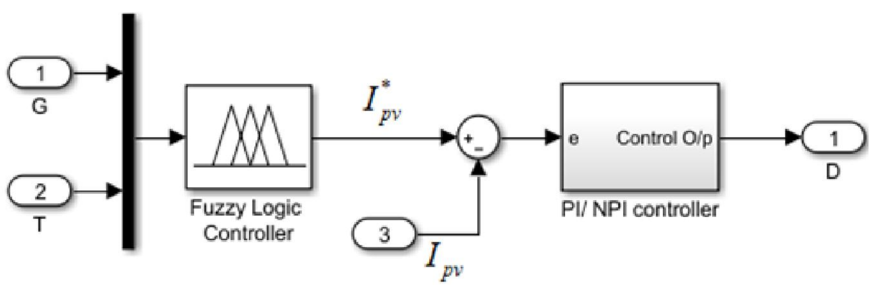

Among several arguments made by researchers, some are listed below which leads to the selection of Ipv as the reference signal for the proposed controller:

1 To enhance the performance of the boost converter, it is crucial to keep the input voltage at a constant value. As the effect of variation in irradiation and temperature over PV array voltage was found to be negligible on this quantity, it couldn't be selected as the reference quantity.

2 Taking PV array power as reference quantity has some setbacks too. If used in absolute form, as the quantity is in kW, the initial error becomes too high, forcing to select higher control gains. On another hand, if used in normalised form, it will lead to non-zero steady-state error due to approximation done via too low scaling factor. Also, selecting a very low scaling factor is a cumbersome process too.

A Sugeno based fuzzy logic system is used with membership functions for irradiance, temperature, and PV current reference as in Figure 12, where linguistic parameters are abbreviated as VL: very low; L: LOW; M: medium; H: high

IJARSCT
International Journal of Advanced Research in Science, Communication and Technology
International Open-Access, Double-Blind, Peer-Reviewed, Refereed, Multidisciplinary Online Journal
ISSN: 2581-9429
Volume 6, Issue 1, July 2026
Impact Factor: 8.2

and VH: very high. The triangular membership function is used to define the variations of the input parameters due to their low-cost digital implementation (Rezk et al., 2019) and ease in fuzzy-logic based arithmetic operations (Kapumpa and Chouhan, 2018).

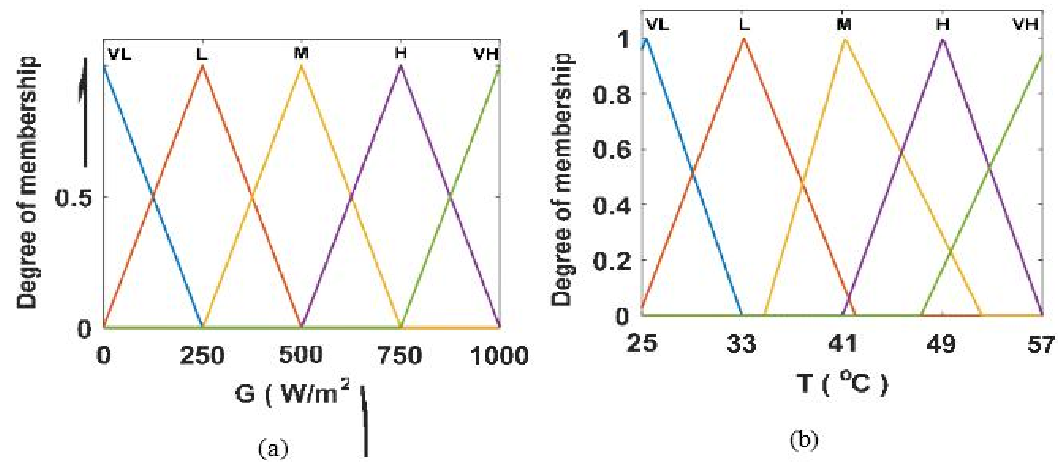

Figure 12 Input membership functions of the proposed controller, (a) irradiance (b) temperature (see online version for colours)

To analyse and verify the crucial role of a controller employed in the proposed optimum power generation algorithms, a performance comparison is carried out using a conventional and improved version of the same controller. A brief discussion on both controllers is provided in the following subsections.

4.1 Fuzzy assisted PI-based (f-PI) optimal power generation method

With the variation in irradiance and/or module temperature, the optimal current reference for the PV array changes as well. A discrete-time PI controller with fixed gains regulates the instantaneous PV Array current to its reference value by processing the error between the two. The control output transfer function in the discrete-time domain is expressed as equation (23):

$$u_{PI}(z) = \left(k_p + \frac{k_i T_s}{z-1} \right) e \tag{23}$$

where e is the error, along proportional gain kp, integral gain ki, and sampling time Ts for the used discrete-PI controller. The controller gains are tuned using the optimisation technique discussed in the later section. The sampling time for the model, in general, can be determined using switching frequency fsw, grid frequency f, and relation (24).

$$T_s = \frac{1}{f_{sw} f} \tag{24}$$

4.2 Fuzzy assisted NPI based optimal power generation method

With large abrupt variation in the irradiation and/or module temperature level, certain sluggish response of the proposed technique could be observed along with large overshoot around the variation instant. One of the main causes of such response is due to the fixed integral gain of the conventional PI controller, causing large controller output when such large error change is experienced. The nonlinear PI (NPI) controller is designed with the main focus on adaptive integral response, which is influenced by the magnitude of error change (Kler et al., 2018a). The control output transfer function of the above PI controller is modified and uses in the given form:

$$u_{NPI}(z) = \left(k_p + \frac{k_i T_s}{z-1} k(e) \right) e \quad (25)$$

where kp, ki are tuned proportional and integral gains, respectively. k(e) is a nonlinear error function represented as:

$$k(e) = \cosh(k_o e) = \frac{\exp(k_o e) + \exp(-k_o e)}{2} \quad (26)$$

V. TEACHING-LEARNING BASED OPTIMISATION

Teaching-learning based optimisation (TLBO) is one of the recent metaheuristic global optimisation algorithm, primitively proposed for the constrained mechanical design problems (Rao et al., 2011). It is inspired by the process following which a student gains knowledge in a conventional classroom environment. In the past few years, this algorithm has attracted great attention from experts and scholars across the globe because, In comparison to other heuristic algorithms, the TLBO has a simplistic implementation, high accuracy, and good convergence capabilities over a wide range of nonlinear platforms (Xue and Wu, 2020). In this context, the TLBO technique is being implemented in the research work for tuning controller gains of a highly nonlinear system like the grid-connected PV system. The detailed process for TLBO implementation is summarised in Figure 11. As can be observed, the TLBO algorithm is segregated into two fundamental parts, i.e., the Teacher phase and learner phase. After the initiation of Np random solutions (collectively known as population), the beginning of a teacher phase is marked by the identification of a solution with the best fitness function value (Teacher).

After that, an attempt to optimise the ith solution from the rest of the population (Students) is made using the following expression:

$$X^{i}_{new} = X^i + r\left(X_{best} - T_F X_{mean}\right) \quad (27)$$

where Xinew, Xi, Xbest and X mean are the new, current, teacher, and mean solution respectively. r is a random number generated within [0,1] and TF is the teaching factor for the teaching phase, generally selected as 1 or 2. If the fitness function of the new solution is found to be lesser than that of the current one, the new solution substitutes the current solution in the student population.

IJARSCT
International Journal of Advanced Research in Science, Communication and Technology
International Open-Access, Double-Blind, Peer-Reviewed, Refereed, Multidisciplinary Online Journal
ISSN: 2581-9429
Volume 6, Issue 1, July 2026
Impact Factor: 8.2

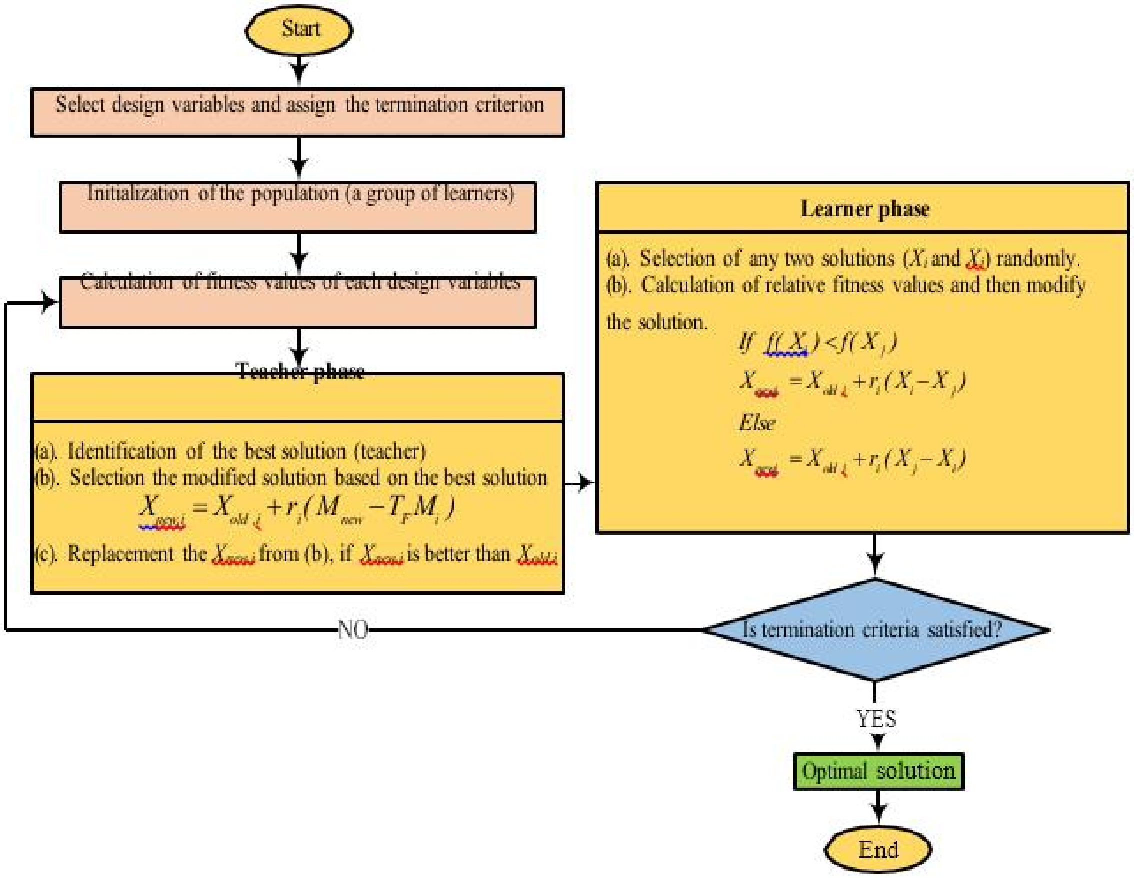

Figure 13 TLBO operational flowchart (see online version for colours)

In contrast to the learner phase, the new solution in the learner phase is determined using the current and a randomly selected solution called as Partner solution Xi:

$$X^i_{new} = X^i + r\left(X^i - X^i_p\right);\ iff\ f\left(X^i\right) < f\left(X^i_p\right)$$
$$or \tag{28}$$
$$X^i_{new} = X^i - r\left(X^i - X^i_p\right);\ iff\ f\left(X^i\right) \geq f\left(X^i_p\right)$$

Similar to the learner phase, if the fitness function value of the new solution is smaller in comparison to the current solution, the new solution replaces the current solution in the population. The first iteration of the algorithm is completed after the same process is repeated for all the students. At the end of each iteration, if the termination criteria is met or the number of iterations performed is equal to the maximum no. of iterations allowed, the training process is terminated.

The cost function for the research project is based upon the weighted sum of the integral of squared error (ISE) and integral of time-weighted absolute error (ITAE), where the error is based upon the normalised reference and instantaneous PV array current. These factors are considered because, among several error classifications, ISE reduces the settling time by eliminating insignificant errors around the reference value whereas ITAE minimises the significant

IJARSCT
International Journal of Advanced Research in Science, Communication and Technology
International Open-Access, Double-Blind, Peer-Reviewed, Refereed, Multidisciplinary Online Journal
ISSN: 2581-9429
Volume 6, Issue 1, July 2026
Impact Factor: 8.2

errors caused by spontaneous and sudden irradiation level variation by regulating transient oscillations. The fitness function (FF) is used to compute the solution cost is formulated in (23) (Wei et al., 2016):

$$FF = b_1 \cdot \left[\int_0^t [e(t)]^2 dt \right] + b_2 \cdot \left[\int_0^t t \cdot |e(t)| dt \right] \quad (29)$$

VI. SIMULATION ANALYSIS

The understudy 100 kW grid-connected PV system is analysed using an illustrative model comprising of SunPower 305E-WHT-U PV array, optimum power generation, and GSC models while using fundamental components from the Simpower systems toolbox of MATLAB/Simulink R2017a. The primary objective is to analyse the performance of the above discussed extant, i.e., P&O and FLC methods as well as proposed fuzzy assisted PI (f-PI) and fuzzy assisted NPI (f-NPI) controllers in terms of overall tracking efficiency, settling time (Ts), and steady-state error (ess) response. A detailed THD analysis is carried out on the three-phase grid current to analyse the effects of variations in the environmental conditions and the impact of proposed and extant controllers in retaining power quality after such deviations occurred. With the frequency of the DC-DC converter and all other relevant subsystems and/or blocks are taken as 5 kHz and grid frequency set to be at 50Hz, equation (24) results in the sampling time for the simulation to be 4 µsec. To demonstrate the superiority of proposed f-PI and f-NPI based optimum power generation methods over the extant controllers, the understudy system is being analysed under three case studies:

Case 1 stepwise variations in irradiance at constant ambient temperature (= 25°C) Case 2 simultaneous stepwise variations in irradiance and ambient temperature Case 3 simultaneous turbulent variations in irradiance and PV module temperature.

6.1 Case 1: Constant temperature and Stepwise irradiance profile

A liquid-cooled PV system, where the surface temperature of the PV array is to be kept constant at standard test condition (STC) (temperature = 25°C) can be an example to realise this case. The irradiance on the PV panel is varied stepwise between 0 and 1,000 W/m2 with an equal step size of 250 W/m2.

For a fair comparison, the gains of the proposed controllers are optimally tuned by TLBO with weight values b1 = 0.6 and b2 = 0.4 as in equation (23), and error defined between Ipv* and Ipv for the 50 iterations. For input parameters (G and T) variation, case-1 is being referred for tuning. Tuning bands under which upper and lower limit of gains were bounded, are, in fact, identical for f-PI and f-NPI controllers and could be expressed as:

$k_p \in [0.1, 20]$, $k_i \in [10, 40]$ and $k_o \in [0, 1]$

The fitness function curves for each controller are provided in Figure 14 while the results are summarised in Table 3 to compare the performance of two proposed controllers in terms of final fitness function values, and the number of iterations taken to converge. Notably, the novel f-NPI based technique could be tuned to converge at a smaller number of iterations in comparison to the proposed f-PI based algorithm, which could be cost-beneficial as the computational time for optimal tuning of the novel controller is reduced. Moreover, with the same number of iterations allowed, if the FF values of two controllers from the above tables could be used to compare the improvement in fitness value using equation (30):

$$\text{Improvement in controller action \%} = \frac{FFvalue_{extant} - FFvalue_{proposed}}{FF\ value_{proposed}}\ 100 \quad (30)$$

then it could be observed that f-NPI outperform f-PI by 16.43% in terms of the overall tracking PV array current to its reference values.

IJARSCT
International Journal of Advanced Research in Science, Communication and Technology
International Open-Access, Double-Blind, Peer-Reviewed, Refereed, Multidisciplinary Online Journal
ISSN: 2581-9429
Volume 6, Issue 1, July 2026
Impact Factor: 8.2

Figure 14 TLBO Fitness function curve for proposed f-PI and f-NPI techniques (see online version for colours)

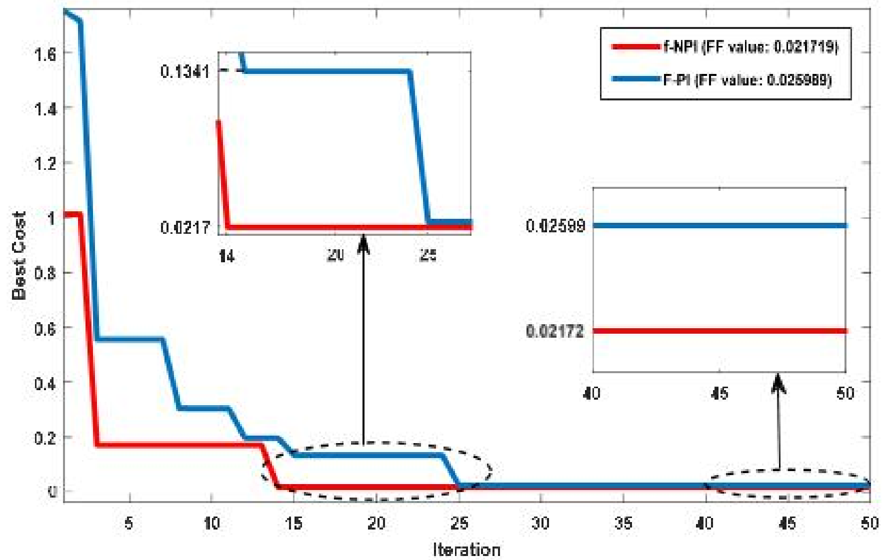

Table 3 Performance comparison of proposed f-PI and f-NPI controllers-based method

Controllers	*Controller gains*			*Fitness function value*	*Number of iterations taken to converge*
	k_p	k_i	k_o		
f-PI	16.296	36.3259	-	0.025989	25
f-NPI	18.680	27.4707	0.7054	0.021719	14

Figure 15 PV system optimal power generation performance for controllers under constant temperature (T = 25°C), (a) variable irradiance with respect to (b) PV array current (c) PV array votlage (d) PV array power (e) PV system output power (see online version for colours)

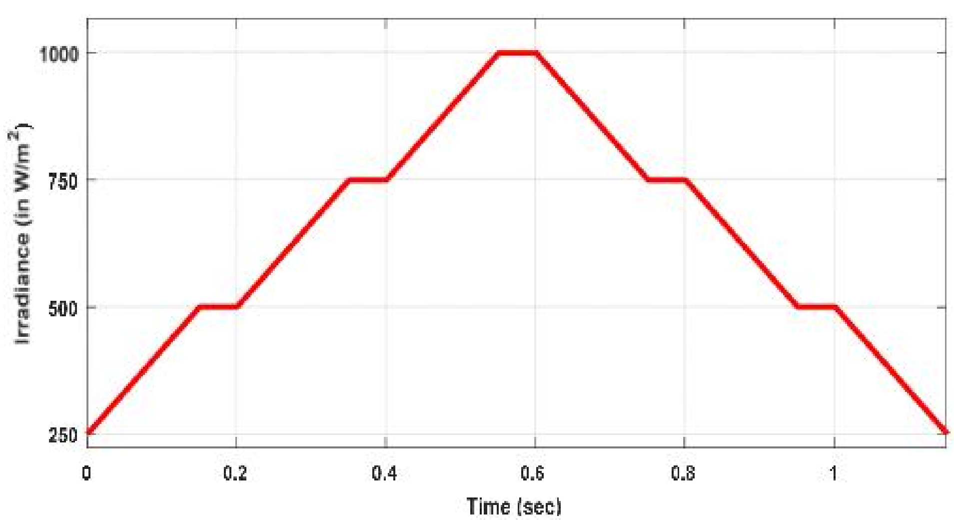

(a)

ISSN: 2581-9429
Impact Factor: 8.2

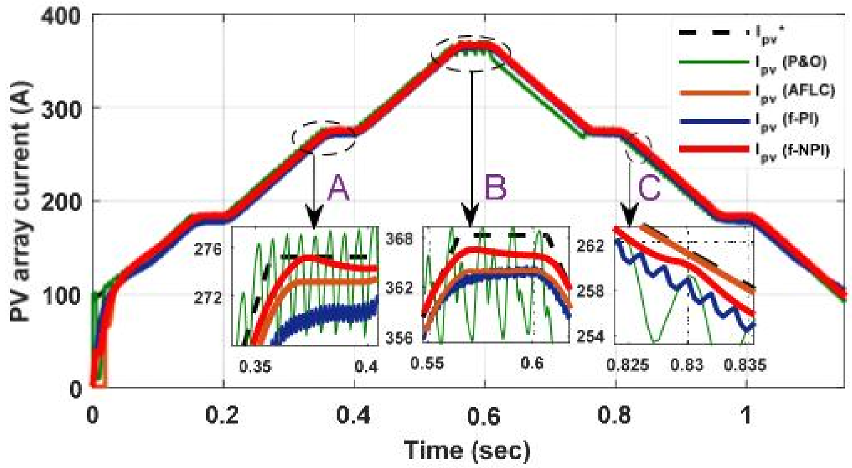

(b)

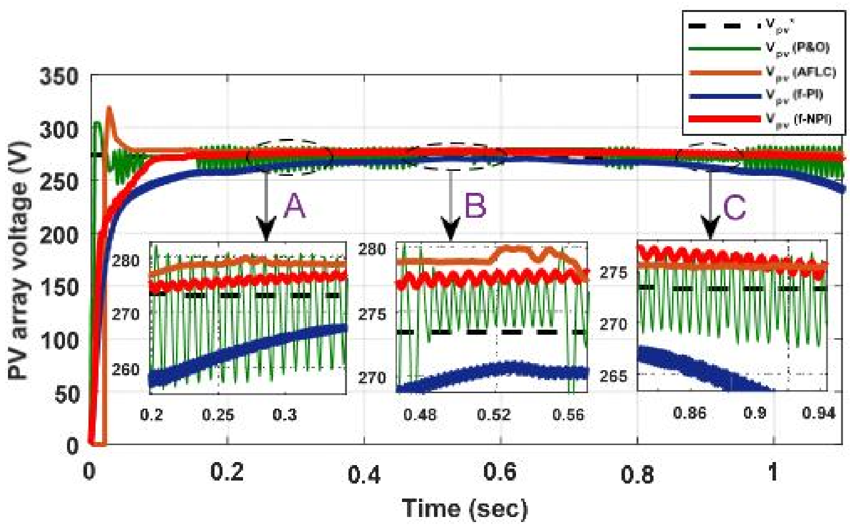

(c)

Figure 15 PV system optimal power generation performance for controllers under constant temperature (T = 25°C), (a) variable irradiance with respect to (b) PV array current
(c) PV array votlage (d) PV array power (e) PV system output power (continued) (see online version for colours)

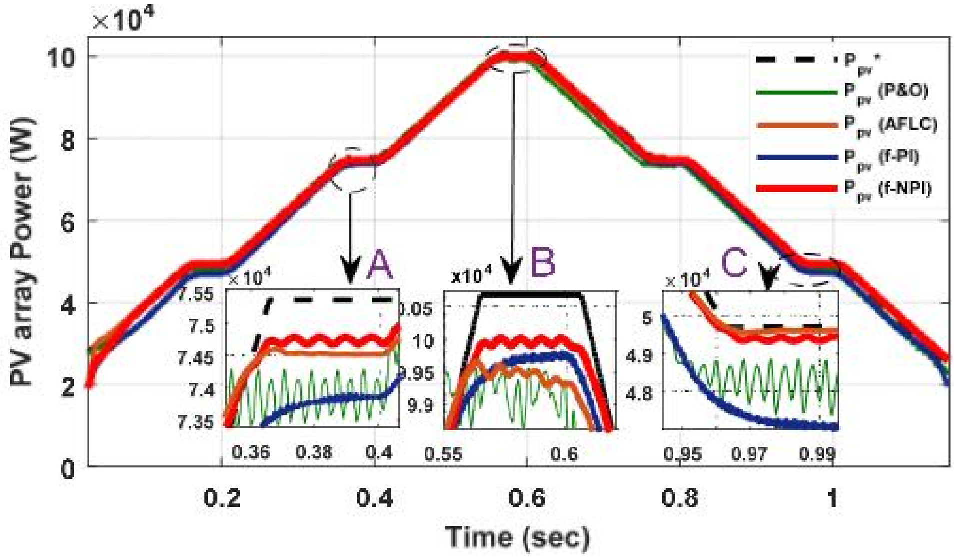

(d)

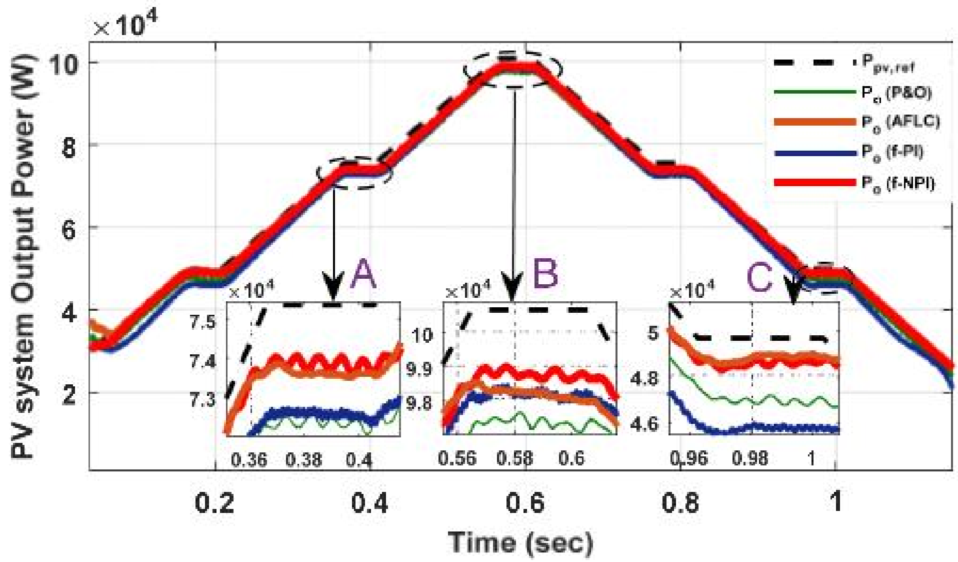

IJARSCT
International Journal of Advanced Research in Science, Communication and Technology
International Open-Access, Double-Blind, Peer-Reviewed, Refereed, Multidisciplinary Online Journal
ISSN: 2581-9429
Volume 6, Issue 1, July 2026
Impact Factor: 8.2

Table 4 Comparative analysis of optimal power methods at different instances in terms of Ppv tracking

Controllers	Instance A			Instance B			Instance C		
	e_{ss} (kW)	T_s (sec)	η% (%)	e_{ss} (kW)	T_s (sec)	η% (%)	e_{ss} (kW)	T_s (sec)	η% (%)
P&O	1.52	0.37	97.98	1.54	0.561	98.47	1.26	0.967	97.46
AFLC	0.83	0.387	98.9	1.23	0.585	98.78	0.05	0.977	99.9
f-PI	1.53	0.386	97.97	0.94	0.587	99.07	2.63	0.994	94.71
f-NPI	*0.66*	*0.366*	*99.12*	*0.72*	*0.572*	*99.28*	*0.32*	*0.966*	*99.36*

The tracking efficiency of the proposed controllers under constant temperature and stepwise irradiation profile [shown in Figure 15(a)] can be analysed via PV array current with respect to its reference value [refer Figure 15(b)] to verify the superior performance of the proposed f-NPI controller around almost all instances. The tracking performance of each controller is also summarised in Table 4. It can be observed that during instants A and B, the proposed f-NPI (fuzzy supervised NPI) outperforms the other techniques in terms of steady-state error (ESS) minimisation and steady-state efficiency. At instant A, the steady-state errors offered by P&O and adaptive fuzzy logic controller (AFLC) based methods are 56.57% and 20.482% greater than that of f-NPI based controller respectively. In terms of settling time, the proposed f-NPI based techniques converge faster to the optimal power point in comparison to P&O and AFLC by 1.21% and 5.556% respectively. Furthermore, in some instances, superior performance of the proposed f-PI based optimal power method could be observed next to the f-NPI controller (refer to Instant B). In such instances, the f-PI based optimal power method generates power at an operating efficiency of about 0.596% and 0.287% greater than that of extant P&O and AFLC techniques respectively.

During the simulative analysis, there are some rare instances (refer instance C) where the extant AFLC provides high-quality tracking performance in comparison to the proposed controllers. However, it is to be noted that similar to the random dataset recorded in Table 4, the majority of instances indicate that the f-NPI based optimal power generation operation averaged over the full operational cycle, will be the most economical choice in comparison to other discussed controller. From Figure 15(c), it is observed that PV array voltage is within the bounds of design assumption for boost converter for different irradiances taken in sub-section 2.2. Figure 15(d) shows PV system output power variation, injecting into the grid, where the proposed controller is again proven to have superior tracking efficiency in terms of tracking speed and steady-state error.

6.2 Case 2: Stepwise temperature and irradiance profile

This case is a more generalised and common scenario faced by PV systems installations where no cooling method is provided. Also, the variation of temperature and solar radiation [refer to Figures 16(a) and 16(b)] is assumed to be proportional with nonlinearly step size throughout the operational cycle.

Figure 16(c)-16(e) shows the system variable tracking performance of the extant and proposed controllers under the second case-study. PV array current tracking performanceshown in Figure 16(c) indicates to the superior performance of the proposed f-NPI controller over others at all instances. Moreover, the PV array voltage oscillations observed in this case study with P&O technique [refer to Figure 16(d)] are even higher than that of the previous case, due to which rating of the DC-DC converter will likely to increase along with the effective size and the initial cost of installation for the grid-connected SPV system if P&O method is employed for optimal power generation. Figure 16(e) shows the variation in PV system output power at the grid terminal, with the instantaneous value of PV array power considered as the reference signal to compare the overall efficiency of different controllers.

ISSN: 2581-9429
Volume 6, Issue 1, July 2026
Impact Factor: 8.2

Figure 16 PV system optimal power generation performance for controllers under simultaneous stepwise variation in (a) irradiation and (b) module temperature with respect to –
(c) PV array current (d) PV array voltage (e) PV system output power with reference to instantaneous PV array power (see online version for colours)

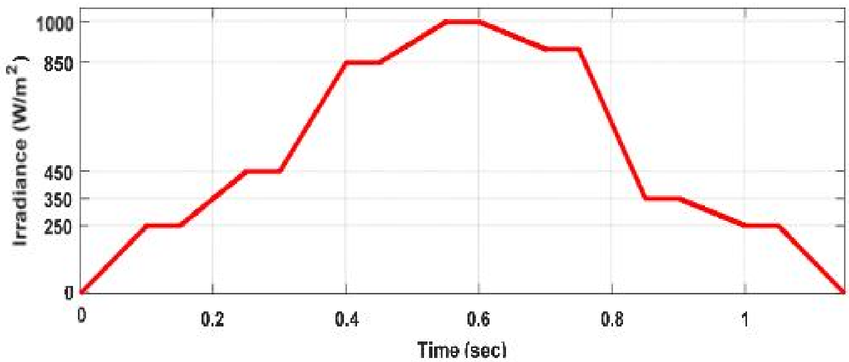

(a)

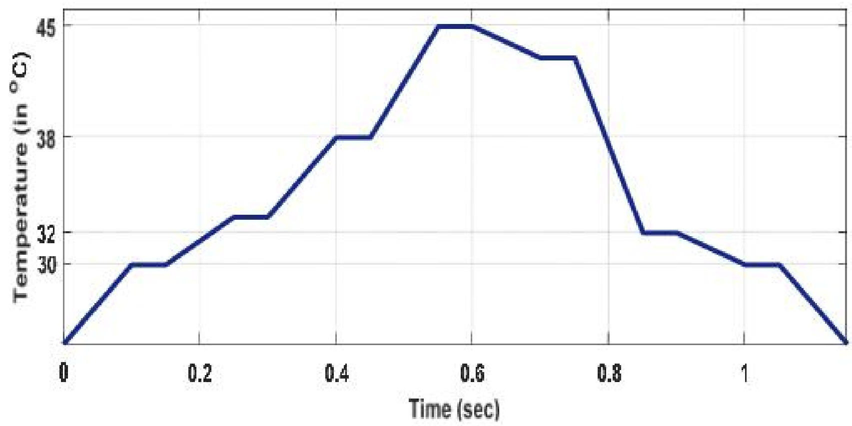

(b)

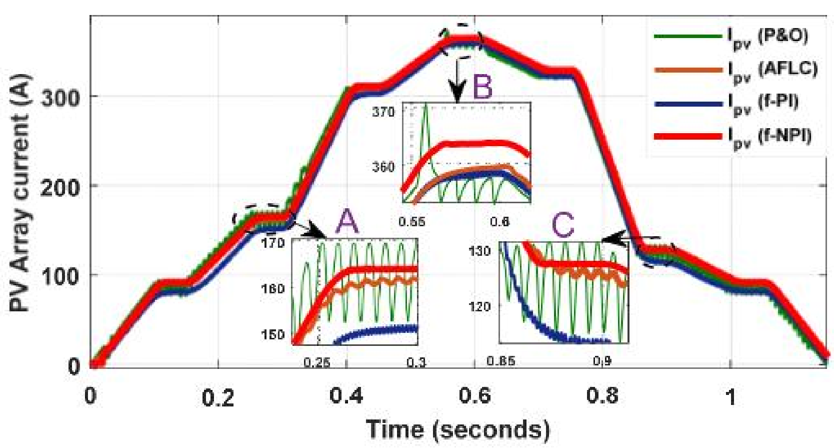

DOI: 10.48175/IJARSCT-37663

IJARSCT
International Journal of Advanced Research in Science, Communication and Technology
International Open-Access, Double-Blind, Peer-Reviewed, Refereed, Multidisciplinary Online Journal
ISSN: 2581-9429
Volume 6, Issue 1, July 2026
Impact Factor: 8.2

Figure 16 PV system optimal power generation performance for controllers under simultaneous stepwise variation in (a) irradiation and (b) module temperature with respect to –
(c) PV array current (d) PV array voltage (e) PV system output power with reference to instantaneous PV array power (continued) (see online version for colours)

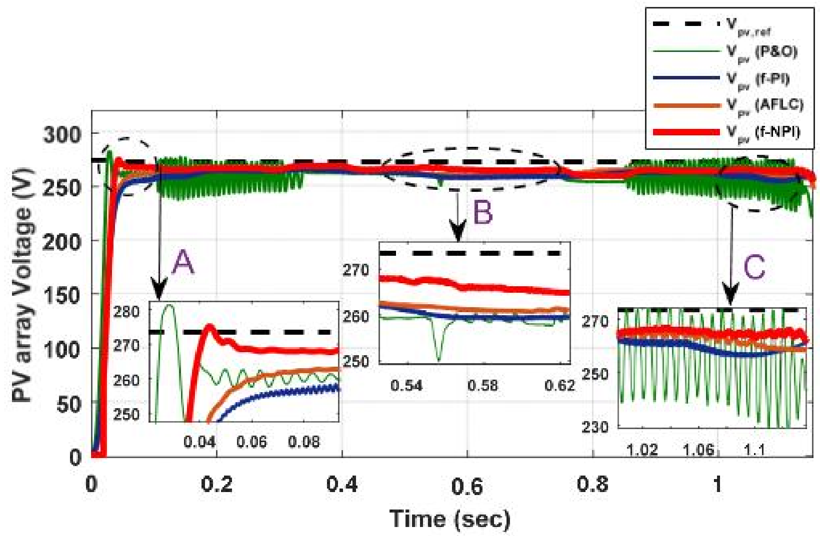

(d)

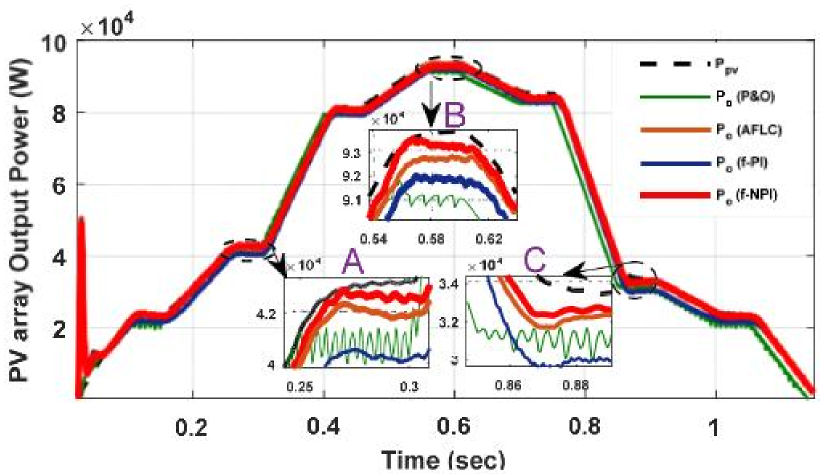

(e)

It is evident from Table 5 that the steady-state error of the SPV output power due to converter operation using extant P&O & AFLC methods is 1.83 kW and 0.78 kW higher than the steady-state error offered by the proposed f-NPI based optimal power generation technique respectively. With the proposed f-NPI based method, the settling time of optimal power point tracking has been reduced by 3 msec. and 7 msec. in comparison to extant P&O and AFLC method respectively. Furthermore, the highest recorded converter tracking efficiency of the proposed f-NPI controller is 99.46%, which is 2.51% and 0.5% higher than the recorded maximum efficiency of P&O and AFLC methods respectively. It implies that if the proposed f-NPI controller is utilised, the rate of power generated can be up to 252.75

IJARSCT
International Journal of Advanced Research in Science, Communication and Technology
International Open-Access, Double-Blind, Peer-Reviewed, Refereed, Multidisciplinary Online Journal
ISSN: 2581-9429 Volume 6, Issue 1, July 2026 Impact Factor: 8.2

W per 0.05sec. and 50.35 W per 0.05 sec. higher than that of extant P&O and AFLC controllers for a 100.7 kW SPV system respectively.

Table 5 Performance comparison of optimal power methods for different instances in terms of SPV system output power (Po) tracking

Controllers	Instance A			Instance B			Instance C		
	e_{ss} (kW)	T_s (sec)	η% (%)	e_{ss} (kW)	T_s (sec)	η% (%)	e_{ss} (kW)	T_s (sec)	η% (%)
P&O	2.28	0.261	94.72	2.86	0.579	96.95	2.24	0.878	93.28
AFLC	1.23	0.29	97.15	1.07	0.584	98.86	1.37	0.895	95.93
f-PI	2.81	0.286	93.48	1.88	0.591	97.92	3.32	0.742	90.04
f-NPI	*0.45*	*0.284*	*98.96*	*0.51*	*0.582*	*99.46*	*0.95*	*0.888*	*97.18*

6.3 Case 3: Turbulent temperature and irradiance profile

To validate the performance of the proposed controller in terms of adaptivity and robustness against uncertain input parameters variation, this case study is conducted under the turbulent temperature and irradiance profile shown in Figures 17(a) and 17(b) respectively. The base dataset comprising of recorded Monthly mean daily global radiation (G in MJ/m2) and Monthly mean daily ambient temperature (Ta in OC) is being collected from the Indian Meteorological Department (IMD) for the New Delhi IMD station (Tyagi, 2009). Unfortunately, the radiation data are generally measured by thermoelectric pyranometers, which are scheduled to be calibrated once a year as per the world radiometric reference (WRR) (Rohilla and Singh, 2020). The PV module temperature is then estimated using Ross Model, relating Cell Temperature (Tc), instantaneous irradiance (G), and ambient temperature (Ta) via Equation (A1) (Sun et al., 2020):

$$T_c = T_a + (T_{noct} - 20)\,\frac{G}{800} \tag{31}$$

where the normal operating cell temperature is taken as (Sun et al., 2020). At last, constrained turbulence is introduced into the base input parameters data via Band-Limited white noise generator with Noise power of 25 and 0.012 for Irradiance and temperature profile respectively. The sample time for both noise generators is kept the same at 8 msec. to ensure proportionate variations in both parameters.

Figures 17(c)–17(e) represents the tracking performance of extant and proposed controllers in terms of SPV system state parameters variations under case study 3. As expected, the proposed f-NPI controller outperforms extant and proposed f-PI controller at almost all instances in an operational cycle. The proposed fuzzy controllers succeed in adapting to the turbulent input profile as those provide satisfactory response with high robustness and accuracy. However, as one could observe in Figure 17(e), the optimum power generation via conventional P&O method with fixed perturbation step for duty cycle leads to great loss in comparison to other controllers. Furthermore, the magnitude of oscillations in PV array terminal voltage [refer to Figure 17(d)] observed with the P&O method is quite large, due to which the converter can face eminent electrical damage if the operation with P&O method is allowed for an extended duration of time.

IJARSCT
International Journal of Advanced Research in Science, Communication and Technology
International Open-Access, Double-Blind, Peer-Reviewed, Refereed, Multidisciplinary Online Journal
ISSN: 2581-9429
Volume 6, Issue 1, July 2026
Impact Factor: 8.2

Figure 17 PV system optimal power generation performance for controllers under simultaneous turbulent variation in (a) irradiation and (b) module temperature with respect to –
(c) PV array current (d) PV array voltage (e) PV system output power with reference to instantaneous PV array power (see online version for colours)

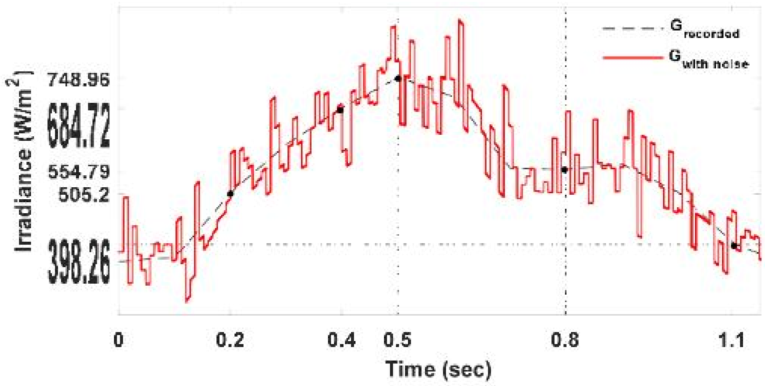

(a)

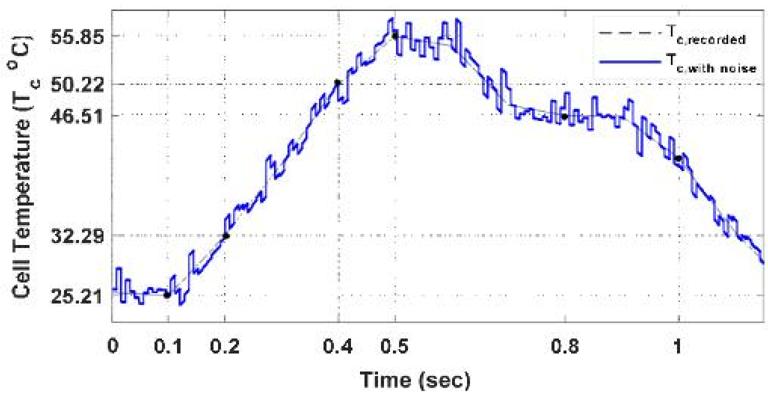

(b)

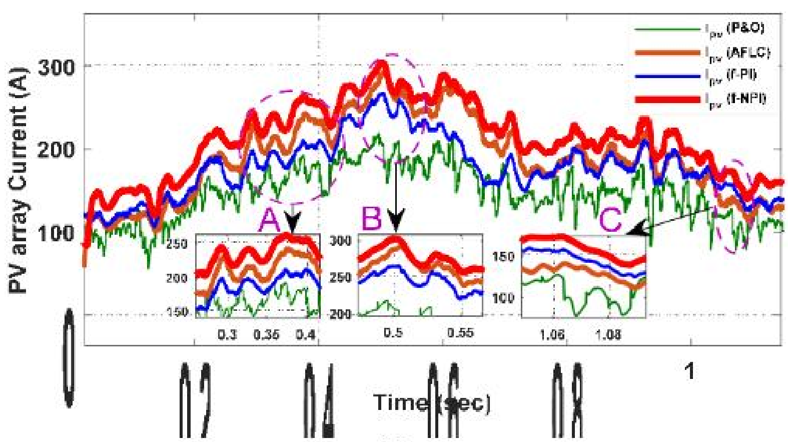

(c)

DOI: 10.48175/IJARSCT-37663

IJARSCT
International Journal of Advanced Research in Science, Communication and Technology
International Open-Access, Double-Blind, Peer-Reviewed, Refereed, Multidisciplinary Online Journal
ISSN: 2581-9429
Volume 6, Issue 1, July 2026
Impact Factor: 8.2

Figure 17 PV system optimal power generation performance for controllers under simultaneous turbulent variation in (a) irradiation and (b) module temperature with respect to –
(c) PV array current (d) PV array voltage (e) PV system output power with reference to instantaneous PV array power (continued)(see online version for colours)

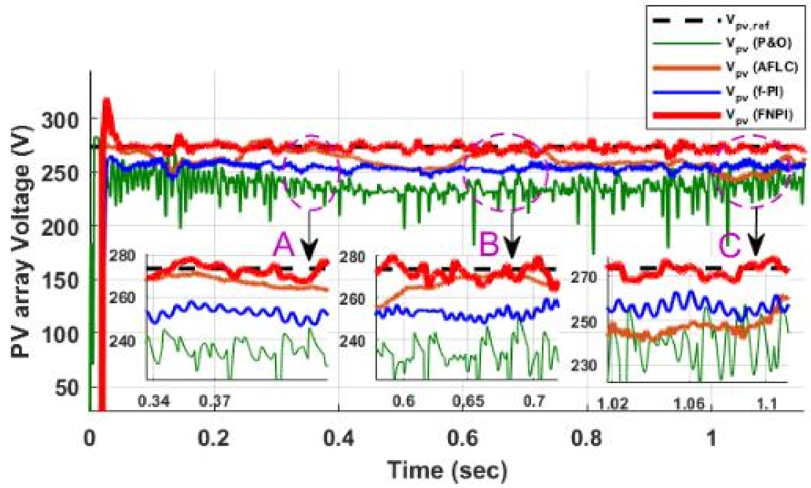

(d)

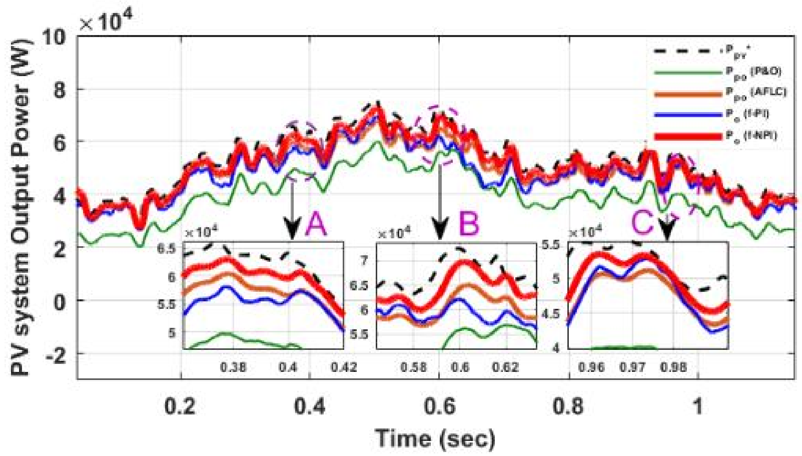

(e)

Similar to case-1 and case-2, there are some instances [refer Instance C, Figure 17(e)], where the proposed f-PI controller manages to provide superior performance in comparison to the extant AFLC controller in terms of reference current tracking [Figure 17(c)] and converter efficiency.

Figure 18 represents the proposed f-NPI controller-based inverter three-phase output current, which is fed into the utility grid. The THD analysis of extant, as well as proposed controllers under environmental conditions and instances, stated in case-1 and case-2 are summarised in Table 6. The THD values are calculated with respect to phase-a current for three cycles and considering frequency components up to 1,000 Hz. As could be observed, THD analysis has shown similar results as seen so far, i.e., proposed f-NPI based controller outperforms other controllers at almost every instant in both cases, with improvement approximately in between 0.53%–4.67%. Similar to the previous analysis, the proposed f-PI outperforms extant AFLC in some instances (Case-1, Instance A, and Case-2, Instance C) in terms of

IJARSCT
International Journal of Advanced Research in Science, Communication and Technology
International Open-Access, Double-Blind, Peer-Reviewed, Refereed, Multidisciplinary Online Journal
ISSN: 2581-9429
Volume 6, Issue 1, July 2026
Impact Factor: 8.2

THD content in the inverter current. In additions, it can be observed that the performance of f-NPI under the case-2 study falls under compliance of IEEE 929 standard (Pandey et al., 2018) for geographical locations with medium to high irradiance level (instances A & B) with harmonics considered from 3rd to 9th components of the fundamental frequency.

Figure 18 Three-phase PV inverter current with proposed f-NPI controller under (a) Case-1 and (b) Case-2 environmental input variations (see online version for colours)

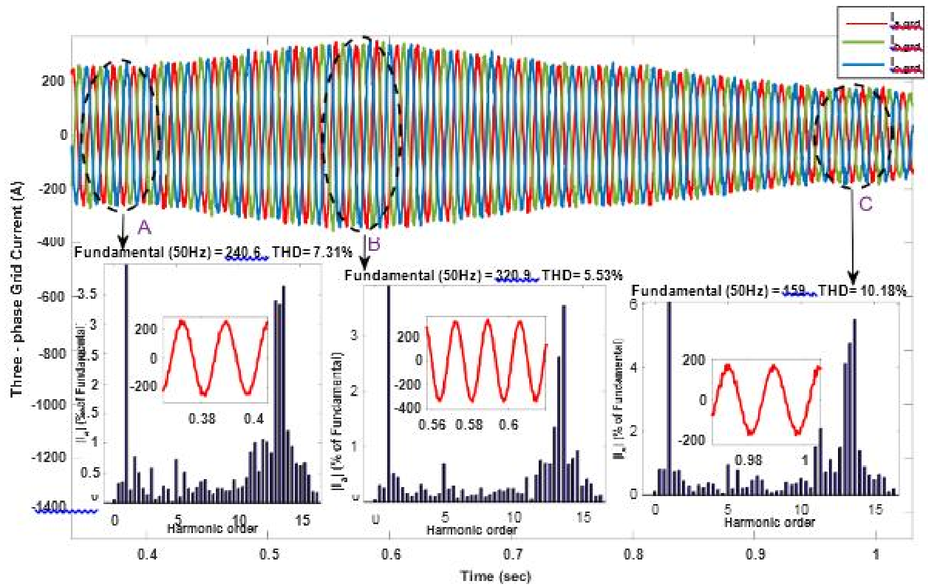

(a)

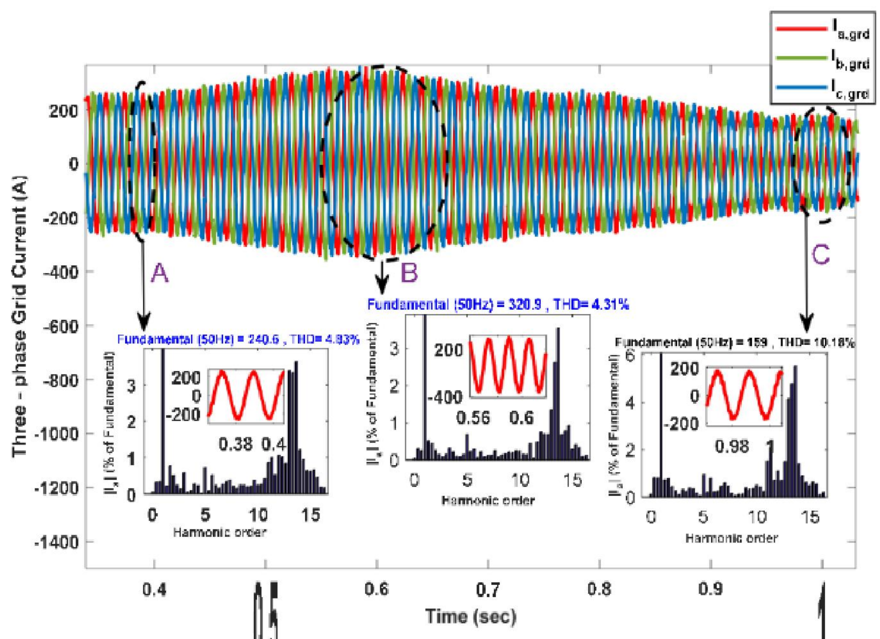

(b)

DOI: 10.48175/IJARSCT-37663

Table 6 THD magnitude (in %) at different instances under case-1 and case-2 environmental variation

Controllers	Case-1 (25°C and variable irradiance)			Case-2 (variable temperature and irradiance)		
	A	B	C	A	B	C
P&O	6.07	5.78	14.85	7.27	5.66	10.71
AFLC	5.12	7.22	10.24	6.70	5.23	10.39
f-PI	5.80	5.73	14.27	8.01	5.71	10.27
f-NPI	*7.31*	*5.53*	*10.18*	*4.83*	*4.31*	*10.18*

VII CONCLUSIONS

A grid-connected PV system is simulated to access and verify the superior performance of proposed f-NPI based optimal power generation technique over the f-PI, conventional P&O, and extant AFLC methods. In the proposed method, variation in irradiance and temperature are sensed directly to compute reference PV array current using fuzzy logic. The reference PV array current is then compared with its instantaneous value obtained from fuzzy logic and an attempt is made to converge the error within satisfactory levels using PI and NPI controllers. Three case studies are carried out with a constant or variable temperature of PV array as solar irradiance is varied uniformly or non-uniformly to simulate the full extent of an operational cycle. The gain parameters of both controllers are tuned fairly under constant temperature case-study using TLBO. Optimisation results reveal that novel f-NPI based optimal power technique is superior to the proposed f-PI based method in terms of dynamic optimal power tracking and fitness function minimisation by 16.43%.

A comparative analysis reveals that novel f-NPI controller outperforms extant controllers in all case studies at almost every instant of operation, with overall tracking efficiency ranging from 97.18% to 99.46%. The simulation results enable the reader to observe high oscillation operation of the conventional P&O method (efficiency in between 93% to 98%), which hence to be considered inferior to the f-PI controller (90%–99% efficiency), which entails almost same level of optimal power tracking capabilities with much considerably fewer oscillations.

A THD analysis is carried out to analyse the impact of the proposed and extant controller on the power quality of three-phase current fed into the utility grid. It is evident from the observations that the f-NPI based optimal power generation controller implementations have inverter a.c. current with superior power quality than any other discussed controllers; with enhancement found to be in the range of 0.53%–4.67%. Moreover, the power quality of utility grid current is found to be within IEEE 929 standards in some instances for the proposed f-NPI based controller operating under simultaneous variation of temperature and irradiance over the grid-interfaced SPV system.

REFERENCES

[1] Adhikari, N. (2018) 'Design of solar photovoltaic energy generation system for off-grid applications', International Journal of Renewable Energy Technology, Vol. 9, Nos. 1/2, p.198.

[2] Adhikari, N., Singh, B. and Vyas, A.L. (2015) 'Design, control and performance analysis of a standalone solar-PV energy generating system', International Journal of Renewable Energy Technology, Vol. 6, No. 1, p.65.

[3] Awadallah, M.A. (2016) 'Identification of partial shading in solar panels using genetic algorithms, simulated annealing, and particle swarm optimisation', International Journal of Renewable Energy Technology, Vol. 7, No. 2, p.125.

[4] Chen, S.Y. (2013) 'Block diagrams and transfer functions of control-to-output and line-to-output for peak current-mode controlled boost converters', IET Power Electronics, Vol. 6, No. 1, pp.60–66.

IJARSCT
International Journal of Advanced Research in Science, Communication and Technology
International Open-Access, Double-Blind, Peer-Reviewed, Refereed, Multidisciplinary Online Journal
ISSN: 2581-9429 Volume 6, Issue 1, July 2026 Impact Factor: 8.2

[5] Chowdhury, M.S., Rahman, K.S., Chowdhury, T., Nuthammachot, N., Techato, K., Akhtaruzzaman, M., Tiong, S.K. et al. (2020) 'An overview of solar photovoltaic panels' end-of-life material recycling', Energy Strategy Reviews, Elsevier Ltd, Vol. 27, Article 100431.

[6] Dash, P.P. and Kazerani, M. (2010) 'Impact of maximum power point tracking on grid-connected photovoltaic system dynamics', CCECE 2010, Calgary, AB, pp.1–5, DOI: 10.1109/ CCECE.2010.5575228.

[7] Elobaid, L.M., Abdelsalam, A.K. and Zakzouk, E.E. (2015) 'Artificial neural network-based photovoltaic maximum power point tracking techniques: a survey', IET Renewable Power Generation, Vol. 9, No. 8, pp.1043–1063.

[8] Fannakh, M., Ehafyani, M.L. and Zouggar, S. (2019) 'Hardware implementation of the fuzzy logic MPPT in an Arduino card using a Simulink support package for PV application', IET Renewable Power Generation, Vol. 13, No. 3, pp.510–518.

[9] Francees, A. and Elshafei, A.L. (2012) 'Maximum power point tracking for wind energy conversion systems based on fuzzy modelling and control', International Journal of Renewable Energy Technology, Vol. 3 No. 1, p.36.

[10] Huang, R., Hong, F. and Ghaderi, D. (2020) 'Sliding mode controller-based e-bike charging station for photovoltaic applications', International Transactions on Electrical Energy Systems, Vol. 30, No. 4, pp.1–25, e12300.

[11] Kapumpa, K.H. and Chouhan, D. (2018) 'A fuzzy logic based MPPT for 1MW standalone solar power plant', 2017 Recent Developments in Control, Automation and Power Engineering, RDCAPE 2017, Vol. 3, pp.153–159.

[12] Kazimierczuk, M.K. (2008) Pulse-Width Modulated DC–DC Power Converters, Wiley, Sussex.

[13] Kler, D., Rana, K.P.S. and Kumar, V. (2018a) 'A nonlinear PID controller based novel maximum power point tracker for PV systems', Journal of the Franklin Institute, Elsevier Ltd, Vol. 355 No. 16, pp.7827–7864.

[14] Kler, D., Sharma, P., Rana, K.P.S. and Kumar, V. (2018b) 'A BSA tuned fractional-order PID controller for enhanced MPPT in a photovoltaic system, fractional order systems', Elsevier Inc., https://doi.org/10.1016/b978-0-12-816152-4.00021-2.

[15] Koizumi, H. and Kurokawa, K. (2005) 'A novel maximum power point tracking method for PV module integrated converter', PESC Record – IEEE Annual Power Electronics Specialists Conference, pp.2081–2086.

[16] Magare, D.B., Sastry, O.S., Gupta, R., Betts, T.R., Gottschalg, R., Kumar, A., Bora, B. et al. (2016) 'Effect of seasonal spectral variations on performance of three different photovoltaic technologies in India', International Journal of Energy and Environmental Engineering, Springer Berlin Heidelberg, Vol. 7, No. 1, pp.93–103.

[17] Malakondareddy, B., Senthil Kumar, S., Ammasai Gounden, N. and Anand, I. (2019) 'An adaptive PI control scheme to balance the neutral-point voltage in a solar PV fed grid connected neutral point clamped inverter', International Journal of Electrical Power and Energy Systems, Elsevier, Vol. 110, No. October, pp.318–331.

[18] Manaullah, N.A., Imbayah, I.I.K. and Ashfaq, H. (2017) 'A controller model for integration of hybrid energy system into the grid', International Journal of Renewable Energy Technology, Vol. 8, Nos. 3/4, p.325.

[19] Messai, A., Mellit, A., Massi, P.A., Guessoum, A. and Mekki, H. (2011) 'FPGA-based implementation of a fuzzy controller (MPPT) for photovoltaic module', Energy Conversion and Management, Elsevier Ltd, Vol. 52, No. 7, pp.2695–2704.

[20] Metry, M., Shadmand, M.B., Balog, R.S. and Abu-Rub, H. (2017) 'MPPT of Photovoltaic Systems Using Sensorless Current-Based Model Predictive Control', IEEE Transactions on Industry Applications, Vol. 53, No. 2, pp.1157–1167.

[21] Mumthas A.J.M. (2018) 'Simulation and analysis of single stage solar PV fed brushless DC motor for water pumping', Int. J. Innovative Research EE, ICE, Vol. 1, Special Issue 2, pp.107–112.

[22] Pandey, S.K., Kumar, S. and Singh, B. (2018) 'Nonadaptive CDSC based control of a single phase PV system tied to distribution grid', India International Conference on Power Electronics, IICPE, IEEE, pp.1–6.

[23] Pathak, P.K. and Yadav, A.K. (2019) 'Design of battery charging circuit through intelligent MPPT using SPV system', Solar Energy, Elsevier, Vol. 178, No. July, pp.79–89.

[24] Rao, R.V., Savsani, V.J. and Vakharia, D.P. (2011) 'Teaching-learning-based optimization: a novel method for constrained mechanical design optimization problems', CAD Computer Aided Design, Elsevier Ltd, Vol. 43, No. 3, pp.303–315.

[25] Renaudineau, H., Donatantonio, F., Fontchastagner, J., Petrone, G., Spagnuolo, G., Martin, J.P. and Pierfederici, S. (2015) 'A PSO-based global MPPT technique for distributed PV power generation', IEEE Transactions on Industrial Electronics, Vol. 62, No. 2, pp.1047–1058.

[26] Rezk, H., Aly, M., Al-Dhaifallah, M. and Shoyama, M. (2019) 'Design and hardware implementation of new adaptive fuzzy logic-based MPPT control method for photovoltaic applications', IEEE Access, Vol. 7, pp.106427–106438, ISSN: 2169-3536, doi: 10.1109/ ACCESS.2019.2932694.

[27] Rohilla, L.N. and Singh, D.K. (2020) 'Direct normal irradiance predictions using broadband models for Indian stations', Energy Reports, Elsevier Ltd, Vol. 6, Supplement, pp.572–576.

[28] Sahoo, J., Samanta, S. and Bhattacharyya, S. (2018) 'Adaptive PID Controller with P&O MPPT Algorithm for Photovoltaic System', IETE Journal of Research, Vol. 2063, https://doi.org/10.1080/03772063.2018.1497552.

[29] Salem, M. and Atia, Y. (2015) 'Control scheme towards enhancing power quality and operational efficiency of single-phase two-stage grid-connected photovoltaic systems', Journal of Electrical Systems and Information Technology, Electronics Research Institute (ERI), Vol. 2, No. 3, pp.314–327.

[30] Singh, P., Shukla, N. and Gaur, P. (2020) 'Modified variable step incremental-conductance MPPT technique for photovoltaic system', International Journal of Information Technology, Springer Singapore, https://doi.org/10.1007/s41870-020-00450-8.

[31] Singh, R., Lakshmanan, S.A. and Rajpurohit', B.S. (2015) 'Performance comparisons of grid connected SPV system with different MPPT algorithms', Int. J. Renewable Energy Technology, Vol. 6 No. 1, pp.84–99.

[32] Sun, V., Asanakham, A., Deethayat, T. and Kiatsiriroat, T. (2020) 'A new method for evaluating nominal operating cell temperature (NOCT) of unglazed photovoltaic thermal module', Energy Reports, Elsevier Ltd, Vol. 6, pp.1029–1042, ISSN 2352-4847 doi: 10.1016/j.egyr.2020.04.026.

[33] Sundareswaran, K., Vigneshkumar, V., Sankar, P., Simon, S.P., Srinivasa Rao Nayak, P. and Palani, S. (2016) 'Development of an improved P&O algorithm assisted through a colony of foraging ants for MPPT in PV system', IEEE Transactions on Industrial Informatics, Vol. 12, No. 1, pp.187–200.

[34] Wei, C., Zhang, Z., Qiao, W. and Qu, L. (2016) 'An adaptive network-based reinforcement learning method for MPPT control of PMSG wind energy conversion systems', IEEE Transactions on Power Electronics, Vol. 31, No. 11, pp.7837–7848.

[35] Xavier, L.S., Cupertino, A.F. and Pereira, H.A. (2018) 'Ancillary services provided by photovoltaic inverters: single and three phase control strategies', Computers and Electrical Engineering, Elsevier Ltd, Vol. 70, pp.102–121, ISSN 0045-7906, doi: 10.1016/j.compeleceng.2018. 03.010.

[36] Xue, R. and Wu, Z. (2020) 'A survey of application and classification on teaching-learning-based optimization algorithm', IEEE Access, IEEE, Vol. 8, pp.1062–1079, ISSN 2169-3536, doi: 10.1109/ACCESS.2019.2960388.

[37] Zhao, B.Y., Zhao, Z.G., Li, Y., Wang, R.Z. and Taylor, R.A. (2019) 'An adaptive PID control method to improve the power tracking performance of solar photovoltaic air-conditioning system', Renewable and Sustainable Energy Reviews, Vol. 113, 109250, ISSN 1364-0321.